Realizing a Space Wi-Fi Link for the ECOsystem Spaceborne Thermal Radiometer Experiment on Space Station (ECOSTRESS) Mission

Michael K. Cheng[*], Dennis K. Lee[*], Josh Miller[†], Vaughn Cable[†], and Bryan Bell[‡]

ABSTRACT. — This article describes the design, analysis, build, and testing of the Wi-Fi telecommunications system for the ECOsystem Spaceborne Thermal Radiometer Experiment on Space Station (ECOSTRESS). The ECOSTRESS payload was successfully installed on the exterior of the space station's Japanese Experimental Module-Exposed Facility (JEM-EF) on July 5, 2018. Due to data rate limitations of the wired connection to the JEM-EF, an IEEE 802.11n Wi-Fi radio was implemented on ECOSTRESS to download payload data via the external wireless network on the average of 27 GB per day. In order to predict the 5.2 GHz Wi-Fi link performance, detailed analysis of the multipath environment outside the International Space Station (ISS) was performed. The ECOSTRESS radio was adapted from a commercial outdoor 802.11n wireless access point that was prescreened and approved by NASA for use on the ISS, in order to ensure compatibility with the external space station Wi-Fi network and to reduce cost. A description of the environmental testing performed on the ECOSTRESS Wi-Fi radio in order to qualify it for operation in space is also provided.

I. Mission Background

The ECOsystem Spaceborne Thermal Radiometer Experiment on Space Station, or ECOSTRESS, is a NASA mission designed to provide critical insight into plant-water dynamics and how ecosystems change with climate [1]. The payload is a 6-band multispectral thermal infrared radiometer covering wavelengths between 8 to 12.5 microns.

The radiometer performs high-resolution measurements of evapotranspiration, which is the sum of evaporation and plant transpiration from the Earth's surface to the atmosphere. These measurements can be used to 1) identify critical thresholds of water use and water stress in key climate-sensitive areas, 2) detect the timing, location, and predictive factors leading to decline and/or cessation of plant water uptake, and 3) determine agricultural water consumptive use to improve drought estimation accuracy over the United States. ECOSTRESS was launched on the Space X Falcon 9 rocket from Canaveral, Florida, on June 29, 2018, and was successfully installed on the International Space Station (ISS) on July 5, 2018.

The ECOSTRESS instrument is located on Site 10 of the Japanese Experimental Module-Exposed Facility (JEM-EF) on the ISS. It is housed in a 1.85 m (L) × 0.8 m (W) × 1.0 m (H) canister. The JEM-EF only provides a 1-Mbps MIL-STD-1553 wired connection that is sufficient for low-rate command and telemetry, but is unable to accommodate the required ECOSTRESS science data volume of about 27 GB/day. Rather than add a faster wired connection to the JEM-EF which would have been difficult and costly, NASA decided to use onboard Wi-Fi to meet the science data collection objectives. Pictures of the JEM-EF, the ECOSTRESS payload, and the Falcon 9 launch vehicle are shown in Figure 1.

The key design requirements [2] for the ECOSTRESS Wi-Fi telecommunications subsystem are as follows:

1. The Telecom Subsystem shall implement wireless IEEE 802.11n Ethernet communications in accordance with the IEEE 802.11 Part 11: Wireless LAN Medium Access Control (MAC) and Physical Layer (PHY) Specifications.
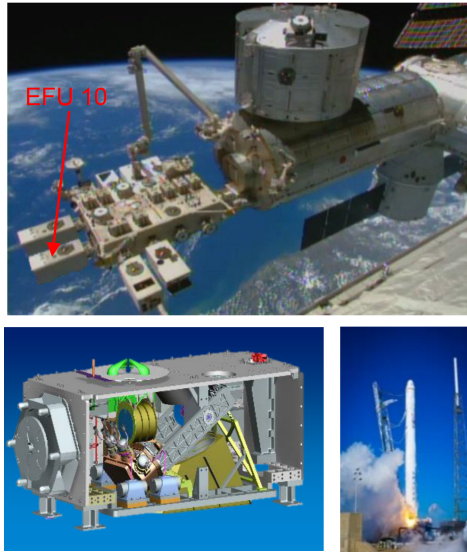
Figure 1. Top: Japanese Experimental Module on the ISS; External Facility Site 10 is identified.
Bottom left: a computer-aided design (CAD) illustration of the ECOSTRESS payload.
Bottom Right: the Space X Falcon 9 launch vehicle.

2. The Telecom Subsystem shall utilize the 5.25–5.35 GHz band for wireless communications.

3. The Telecom Subsystem shall be configured to maximize Radio Frequency (RF) coverage for each radio-to-antenna connection for known ISS structural configurations.

4. The Telecom Subsystem shall be designed to deliver a minimum of −70 dBm signal power as measured at the receiving Wireless Access Points (WAP).

The first two requirements specified that the ECOSTRESS Wi-Fi design had to use the IEEE 802.11n protocol in the 5.2 GHz frequency band. The third requirement was used to maximize the availability of the Wi-Fi link, which was necessary to meet the science data volume return goals. Detailed electromagnetic (EM) modeling were conducted to select optimal antenna placement to maximum RF coverage. The fourth requirement established the minimum signal power threshold needed to maintain the targeted throughput bit rate.

II. ISS External Wi-Fi Network and Dataflow

Prior to the ECOSTRESS mission, NASA had already installed several BelAir 802.11n WAP on the outside of the ISS. However, the closest external WAP to ECOSTRESS was installed on the US Lab module of the ISS and did not provide sufficient coverage for the ECOSTRESS Wi-Fi link. Several other options were considered, including installing a new WAP at the ISS truss or converting the Wi-Fi clients on the External High Definition Cameras (EHDC) into WAPs. The ECOSTRESS project worked together with the ISS to form a set of telecom system requirements that guided the placement of the new WAP and payload antennas. The decision was eventually made to install a new WAP at Node 3 of the ISS in order to support the ECOSTRESS Wi-Fi link. A 3D model of the ISS is given in Figure 2, which shows the ECOSTRESS payload location relative to Node 3.

The ISS Node 3 WAP antennas were installed on handrails (HR) 0606 and 0640. The distance between the HR WAP antennas is approximately 4 meters, and the distance from the ECOSTRESS payload antennas and the HR WAP antennas is approximately 19 meters. The look angles between the payload and ISS Node 3 are shown in Figure 3. The Node 3 antennas are Myers Log-periodic array antennas with linear polarization, a frequency range of 2.4–5.9 GHz, and has a peak gain of 5 dBil. These parameters were used to model the electromagnetic propagation of the external Wi-Fi link.

The ECOSTRESS payload data is compressed using hyperspectral image compression [3] and formed into TCP/IP packets. The TCP/IP packets are sent via the Wi-Fi link to the ISS Node 3 WAP, and then forwarded to a Delay Tolerant Network (DTN) [4] gateway laptop onboard the ISS. The data is stored on the laptop and bundled with payload data from other ISS instruments. When the proper downlink window arrives, the
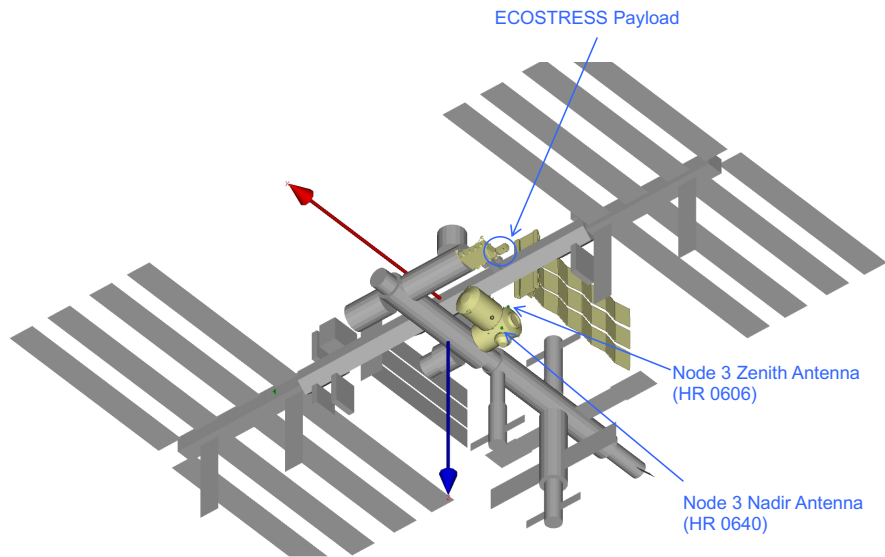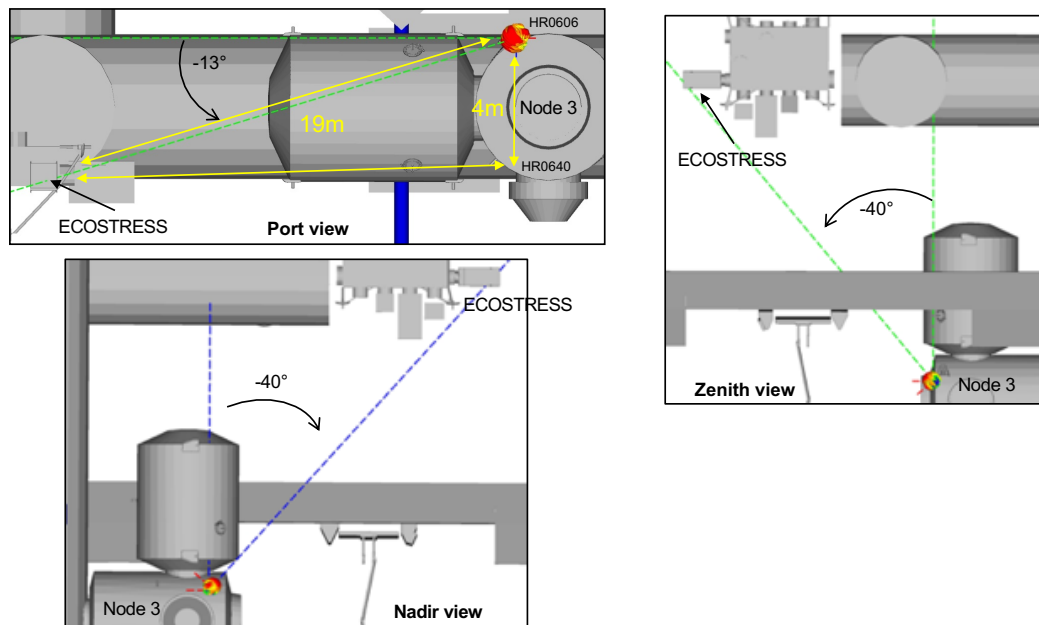
Figure 2. A 3D model of the ISS.

Figure 3. Relative angles between the ECOSTRESS payload and Node 3 (courtesy of Matthew Upanavage, Johnson Space Center). The WAP antennas are located at HR 0606 and 0640.

data is downloaded to Earth via a return link using the NASA Tracking and Data Relay Satellite System (TDRSS). The TDRSS downlink signal is received at the White Sands Complex in New Mexico, and forwarded to the Huntsville Operations Support Center (HOSC) in Alabama. At the HOSC, the data from multiple payloads is ungrouped and forwarded to their appropriate destinations, including to the Jet Propulsion Laboratory (JPL) in Pasadena, California. The science data flow for ECOSTRESS is illustrated in Figure 4.
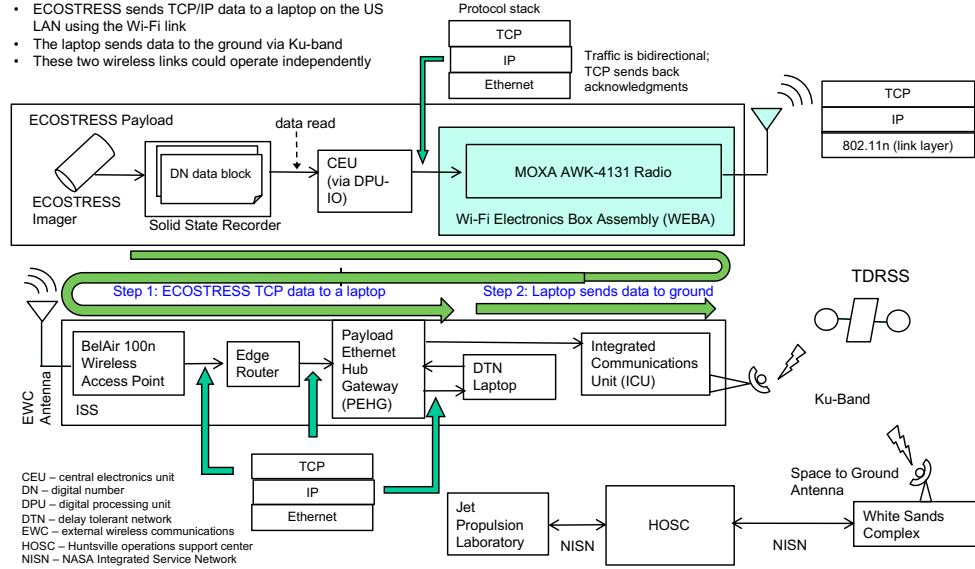

Figure 4. ECOSTRESS science data flow.

III. Link Analysis

This section describes the link analysis performed to ensure that the ECOSTRESS Wi-Fi signal received by the ISS Node 3 WAP met the -70 dBm key requirement (see Section I). Note that the ECOSTRESS payload has two Wi-Fi radios which are each connected to two external Wi-Fi antennas in a top-bottom pairing, and there are also two WAP antennas on Node 3. During operation only one radio is powered on at a time. This resulted in analysis of a total of four different links between the different antennas. The WAP antenna, the payload Wi-Fi antenna, and the locations of the Wi-Fi antennas on the payload are shown in Figure 5.

A. Total Received Power

Due to the mostly metallic surface of the ISS, there are many reflections of the transmitted Wi-Fi signal at the Node 3 receive antenna. These reflections can add constructively or destructively, and result in multipath interference. Ray tracing analysis using the XGtd software was performed by NASA Johnson Space Center (JSC) to calculate the amplitude and phase of the multipath reflections. JPL used these results to compute the
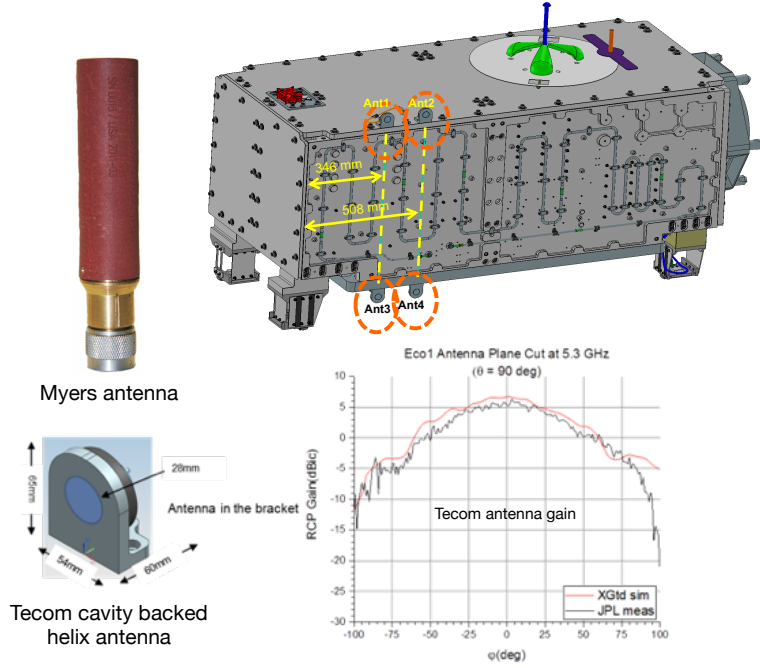
Figure 5. Top left: Myers antenna. Top right: TECOM antenna mounting locations on the ECOSTRESS payload. Bottom left: the TECOM antenna. Bottom right: TECOM antenna gain measurement.

the expected receive Wi-Fi power at Node 3, and to determine the optimum placement of the external antennas at Node 3 to maximize the RF signal strength. The ray tracing outputs were also used to calculate the delay spread of the link to determine if there was multipath inter-symbol interference (ISI).

The vertical plane at each Node 3 antenna was divided into a 0.5 m × 0.5 m grid with a square center-to-square center spacing of 0.1 m as shown in Figure 6. Using the XGtd software, JSC provided the complex impulse response (CIR) of the 25 strongest rays for each square in the grid for each Node 3 antenna. The XGtd simulation parameters are shown in Table 1.

For each square in the receiving grid, the CIR data contained the power x_i (dBm) and the phase θ_i (degrees) for each of the top 25 rays (i=1, 2, $\cdots$, 25). The sum of the top 25 rays in each receiving square can be calculated as shown in the following equation:

$$s = \sum_{i=1}^{25} [10^{(\frac{x_i}{20})} \exp{(j\theta_i)}] \tag{1}$$

Thus, the Total Receive Power (TRP) in each grid square is:

$$\text{TRP} = 20 \log_{10} |s| \tag{2}$$

A list of the TRP in dBm for the 25 strongest rays are given in Table 2. The table headings identify the ECOSTRESS and ISS Node 3 antenna pair being used. ECOSTRESS
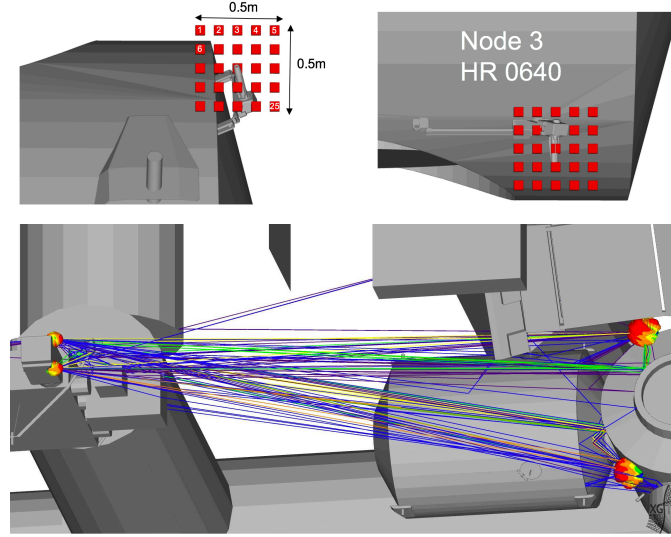
Figure 6. Top left: Node 3 zenith antenna grid. Top right: Node 3 nadir antenna grid. Spacing between squares is 0.1 m. Bottom: the top 25 strongest rays output by XGtd (courtesy of Matthew Upanavage, JSC).

Table 1. XGtd simulation parameters

Structure model	Modified ISS 3R configuration
Propagation model	Full 3D
Ray spacing [deg]	0.25
Reflections [#]	3
Transmissions [#]	0
Wedge diffractions [#]	1
Surface diffractions [#]	1
Ray tracing method	Shooting Bounce Rays
RF frequency [GHz]	5.3
Transmit antenna	Myers log-periodic (vertically polarized)
Transmit cable assembly loss [dB]	15
Transmit power [dBm]	17
Receiver locations	ECOSTRESS – aft face grid 0.05 m spacing
	Node 3 – 0.5 m $\times$ 0.5 m grid
	0.1 m spacing and 0.5 m off surface
Receive antenna	Isotropic (RHCP) – 0 dBic
Receive cable assembly loss [dB]	3
Receiver sensitivity [dBm]	-70

antennas 1 (zenith) and 3 (nadir) are the antenna pairs for the Moxa AWK-4131 Wi-Fi radio board 1, and antennas 2 (zenith) and 4 (nadir) are the antenna pairs for AWK-4131 Wi-Fi radio board 2. The Node 3 zenith antenna is HR0606, and the nadir antenna is HR0640. Using this nomenclature, the column of Table 2 with heading "Eco1_HR0606" represents the wireless link between the zenith antenna for Wi-Fi radio board 1 and the Node 3 zenith antenna.

Table 2. The top 25 strongest rays for each ECOSTRESS-to-Node 3 antenna pair.

| Rx#	Eco1_HR0606 TRP (dBm)	Eco1_HR0640 TRP (dBm)	Eco2_HR0606 TRP (dBm)	Eco2_HR0640 TRP (dBm)	Eco3_HR0606 TRP (dBm)	Eco3_HR0640 TRP (dBm)	Eco4_HR0606 TRP (dBm)	Eco4_HR0640 TRP (dBm)
1	-67.91	-60.99	-65.27	-62.64	-66.51	-68.31	-68.32	-65.44
2	-62.4	-63.65	-62.08	-63.08	-66.54	-64.55	-63.19	-63.7
3	-60.85	-63.85	-61.67	-63.01	-66.57	-67.8	-61.11	-64.34
4	-61.53	-63.87	-63.44	-62.96	-64.01	-67.27	-62.11	-64.48
5	-61.72	-63.54	-62.74	-62.3	-68.28	-67.03	-60.81	-65.98
6	-67.01	-62.11	-69.28	-63.3	-63.37	-80.57	-61.45	-70.03
7	-68.3	-63.11	-65.65	-66.33	-64.37	-74.73	-63.04	-70.74
8	-64.07	-63.43	-60.84	-65.87	-71.17	-71.94	-66.17	-69.1
9	-63.79	-64.1	-60.34	-65.91	-69.21	-71.98	-64.25	-69.79
10	-65.11	-67.1	-61.21	-65.93	-76.04	-66.83	-66.83	-66.85
11	-61.17	-68.98	-60.35	-73.61	-80.98	-64.97	-72.49	-62.53
12	-66.93	-69.81	-76.05	-74.56	-67.43	-64.25	-63.85	-62.76
13	-69.67	-70.55	-69.77	-73.5	-63.88	-64.25	-66.49	-64.02
14	-70.1	-72.86	-65.6	-73.42	-67.91	-64.6	-66.36	-64.62
15	-66.98	-67.16	-64.45	-66.16	-65.01	-67.25	-65.82	-67.43
16	-66.36	-63.19	-64.99	-66.91	-68.08	-74.74	-66.72	-73.19
17	-66.21	-66.64	-61.08	-66.54	-67.84	-77.35	-65.91	-74.23
18	-65.27	-66.08	-64.25	-62.08	-67.43	-79.25	-64.1	-71.53
19	-64.55	-67.32	-64.91	-63.42	-68.77	-71.49	-66.93	-71.34
20	-65.54	-67.85	-65.22	-66.5	-67.02	-67.25	-66.21	-66.81
21	-66.2	-64.35	-66.04	-67.16	-68.06	-66.65	-67.03	-61.81
22	-65.64	-61.58	-65.43	-60.08	-68.97	-65.41	-66	-66.38
23	-65.19	-65.49	-66.55	-64.4	-67.83	-65.57	-64.46	-61.64
24	-66.11	-67.54	-64.1	-65.64	-68.41	-67.34	-66.66	-64.77
25	-66.44	-68.46	-64	-66.1	-67.45	-68.78	-66.55	-67.23

The resulting TRP at the ISS Node 3 zenith and nadir antennas for ECOSTRESS radio board 1 transmitting is shown in Figure 7. Likewise, the TRP for ECOSTRESS radio board 2 transmitting is shown in Figure 8. The TRP results showed that the signal strength could drop by more than 15 dB in adjacent squares due to multipaths. The handrail antenna installation was not exact, so there was a possibility that one or both WAP antennas could be placed in low TRP squares. But this calculation is conservative because it assumes that only a single transmit and a single receive antenna are used. The IEEE 802.11n standard implemented by both the ECOSTRESS Wi-Fi radio and the ISS WAP takes advantage of using multiple antennas to combat multipath fading. Section III.B will describe how antenna diversity and Multiple-Input Multiple-Output (MIMO) processing can improve the TRP of the ECOSTRESS-to-Node 3 link.

B. Antenna Diversity

In single-input single-output (SISO) communication, one transmit antenna is used to communicate with one receive antenna. In this case, the Node 3 antenna installation location on the grid determines the link TRP as given by the heat maps of Figure 7 and Figure 8. However, each AWK-4131 board in the ECOSTRESS radio transmits by using two antennas; the Node 3 WAP also has two antennas. Both the ECOSTRESS and ISS WAP radios support the IEEE 802.11n standard that utilizes antenna diversity to achieve MIMO communications and increase signal strength and throughput. Two straightforward diversity approaches, selection combining and equal gain combining, were considered in the multipath analysis to see how they could boost link margin. Since the primary operational mode is for ECOSTRESS to upload science data to the WAP, the analysis assumes that the Node 3 WAP radio will combine the use of both
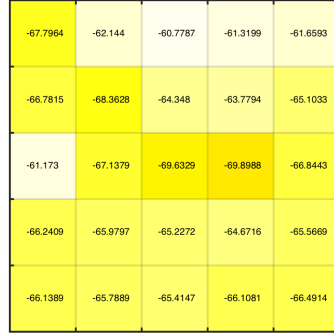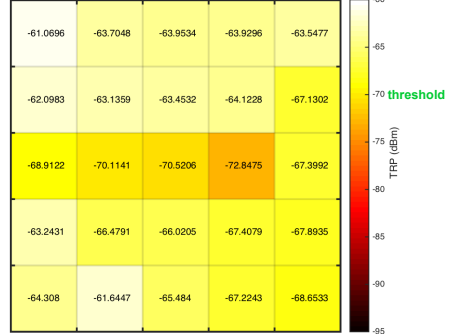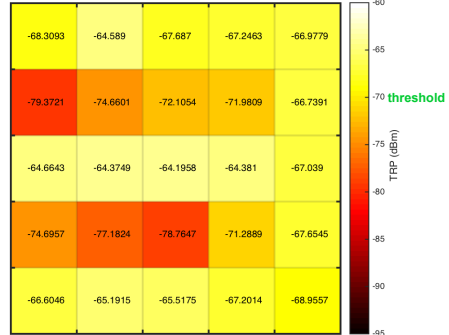
Figure 7. Total received power for ECOSTRESS radio board 1 to ISS Node 3 antenna links.
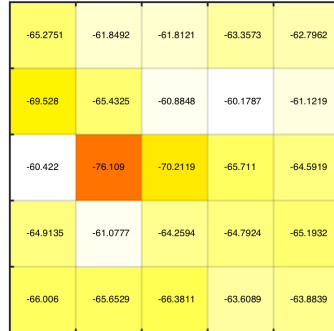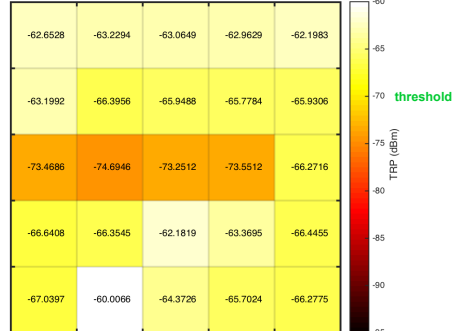
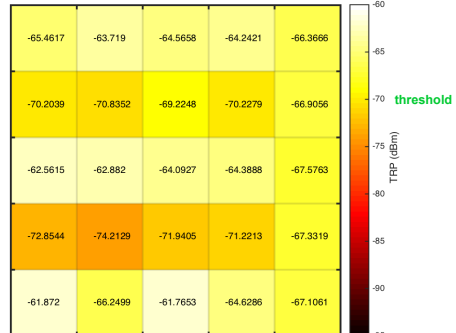**Figure 8. Total received power for ECOSTRESS radio board 2 to ISS Node 3 antenna links.**

of its antennas whenever possible. Although information about the exact algorithms used by the commerical-off-the-shelf (COTS) Wi-Fi radios on how and when to employ antenna diversity was not available, Section V will show throughput results of field testing that if conditions allow, both radios will indeed utilize multiple antennas to increase the received power and the overall data throughput. While single antenna analysis indicated that, in some cases, the Wi-Fi link did not meet the TRP requirement, further refinement of the multipath analysis to include antenna diversity boosted the predicted TRP well above the MIMO threshold and met the required link margin for the targeted throughput rate.

1. Selection Combining

With one transmit antenna and multiple receive antennas, selection combining picks the receive antenna that gives the strongest receive signal strength. An illustration of selection combining is given in Figure 9. For the ECOSTRESS Wi-Fi link, there are two transmit antennas and two receive antennas. For each payload transmit antenna, there are two receiving grids (zenith and nadir) at ISS Node 3. Since each grid has 25 location squares, there are 625 (zenith, nadir) pairs for each payload transmit antenna. Selection combining uses the highest powered link so there are 625 maximum TRP values corresponding to the 625 antenna pairings. A distribution of these TRP values using selection combining is plotted in Figure 11.
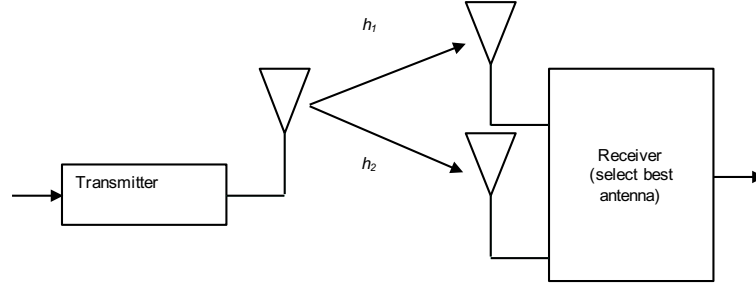

Figure 9. MIMO – selection combining.

2. Equal Gain Combining

Rather than discarding the weaker received signals as done in selection combining, the received signals can be scaled, phase aligned, and summed together to increase the overall received signal strength. An illustration of this approach is given in Figure 10. If the amplitude scale factor is unity for all antennas, the approach is named equal gain combining. If the scale factor is proportional to the channel gain h_i, the approach is called maximal ratio combining. Maximal ratio combining provides improved performance over equal gain combining, but requires the receiver to estimate and adapt the channel gain to the wireless environment. In both cases, the signals from the receive antennas must be phase rotated and aligned to ensure that the signals sum coherently.

To calculate the TRP using equal gain combining, the sum signal in each grid square
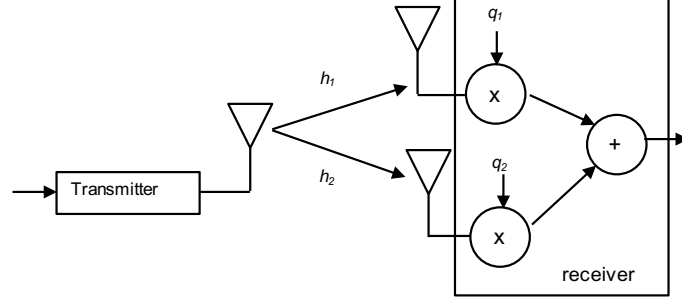
Figure 10. MIMO – equal gain combining

for each Node 3 WAP antenna is computed using Equation. 1. Then for each payload transmit antenna, the sum signals from corresponding squares in the zenith and nadir antenna grids at Node 3, $s_{zenith,l}$ and $s_{nadir,l}$ respectively, are combined as follows to obtain the TPR with equal gain combining:

$$\text{TRP}_l = 20 \log_{10} \left(|s_{zenith,l}| + |s_{nadir,l}| \right) \tag{3}$$

Index l ranges from 1 to 625, one for each Node 3 (zenith, nadir) antenna square pairing described earlier. A distribution of the received powers for equal gain combining is plotted in Figure 11.
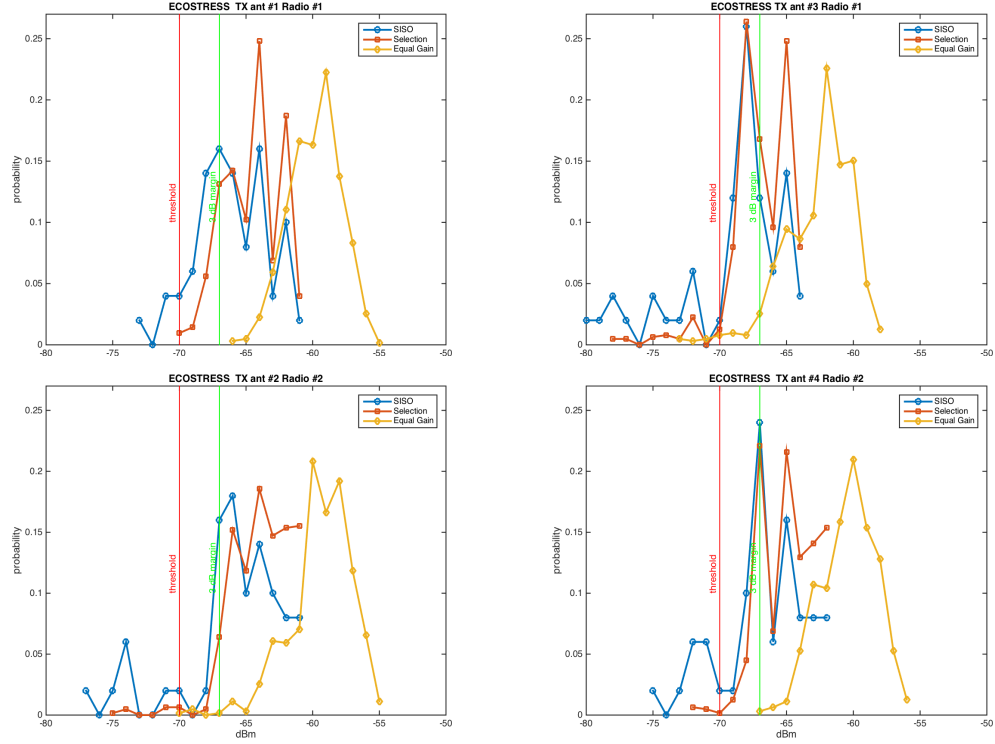

Figure 11. Comparing TRP distributions for different antenna diversity schemes.

From the distributions in Figure 11, the probability of meeting a specific power threshold for each Wi-Fi radio board and each combining scheme was computed with results shown in Table 3. For each payload radio board #1 or #2, there are two transmit antennas. The ECOSTRESS Wi-Fi radio board #1 is connected to antennas TX1 and TX3. The ECOSTRESS Wi-Fi radio board #2 is connected to antennas TX2 and TX4. For each combining scheme and each Wi-Fi radio board, there are two columns in Table 3 – one for each TX antenna. As the table shows, the probability of closing the link with a 3 dB margin is higher with selection combining and even higher with equal gain combining. The results show that MIMO antenna diversity does provide significant performance improvement in the Wi-Fi link for ECOSTRESS.

Table 3. Combined Radio Coverage.

| Probability of a 3dB margin over -70 dBm	SISO		Selection Combining		Equal Gain Combining	
	TX ant1/ant2	TX ant3/ant4	TX ant1/ant2	TX ant3/ant4	TX ant1/ant2	TX ant3/ant4
Radio #1	0.70	0.36	0.92	0.59	1.00	0.96
Radio #2	0.84	0.70	0.98	0.93	0.99	1.00

C. Delay Spread

Having sufficient TRP alone cannot guarantee robust Wi-Fi communications. Analysis was also performed to make sure that ISI due to multipaths did not pose a problem for the Node 3 link. To verify this, the delay spreads of the Wi-Fi channel under different conditions were computed and compared to the inter-symbol guard time of the Wi-Fi transmitter.

The XGtd ray tracing simulations by JSC also provided the arrival time of the top 25 rays for each antenna pair. Excess delay is computed as the difference in the arrival time of the ith ray compared to the first received ray. If there was a line of sight (LOS) path between the transmitter and the receiver, the direct LOS ray was the first received ray. The power delay profile (PDP) is defined as the channel power spectral density as a function of delay; namely, how "channel power" is distributed as a function of the excess delay. To avoid ISI, the channel power of each symbol should be confined within that symbol period and the guard interval, and not spread into neighboring symbols. A sample PDP of the top 25 rays between ECOSTRESS and Node 3 is given in Figure 12. Note that the maximum receiver sensitivity for the Moxa radio is −100 dBm, so only those rays above this threshold are shown.

From the power delay profile, the delay spread was computed over the i strongest rays in the following sequence, where τ_i is the excess delay of the ith ray. The mean excess delay (or the first moment of the power delay profile) $\bar{\tau}$ is given by:

$$\bar{\tau} = \frac{\sum_i P(\tau_i)\tau_i}{\sum_i P(\tau_i)}. \tag{4}$$
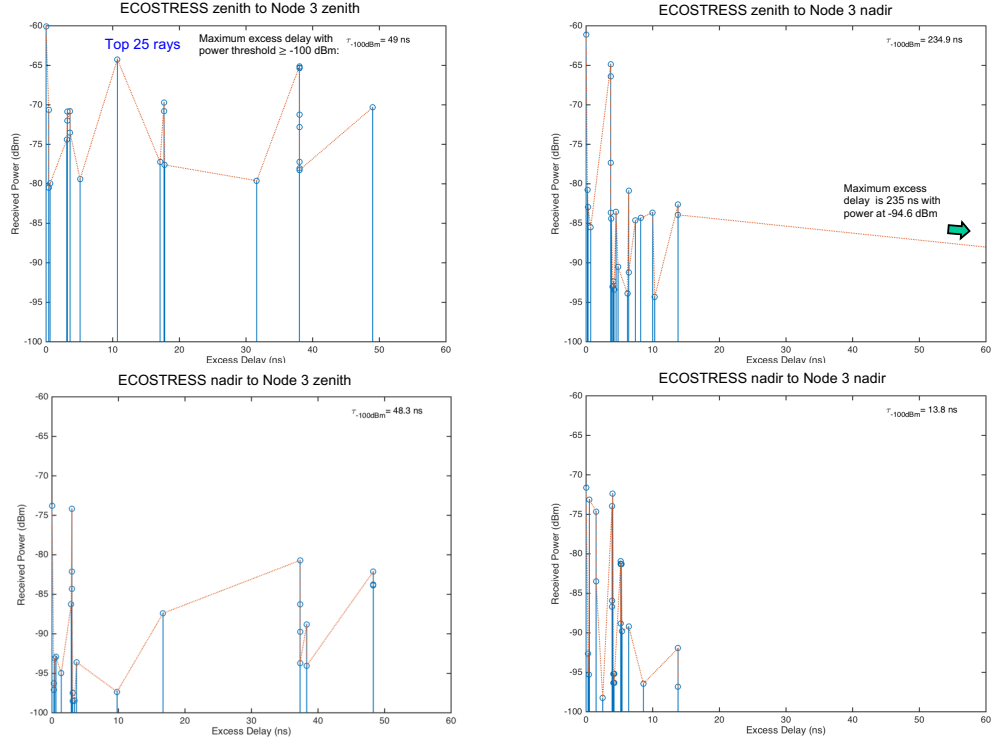
Figure 12. Power delay profile for the Wi-Fi link between ECOSTRESS and Node 3.

The second moment of the delay profile, $\bar{\tau}^2$, is given by:

$$\bar{\tau}^2 = \frac{\sum_i P(\tau_i)\tau_i^2}{\sum_i P(\tau_i)}. \tag{5}$$

The first and second moments of the PDP are used to compute the root mean square (RMS) delay spread as follows:

$$\sigma_\tau = \sqrt{\bar{\tau}^2 - (\bar{\tau})^2}. \tag{6}$$

The computed values for each ECOSTRESS-to-Node 3 antenna pair given in Table 4 used Equations 4, 5, and 6, and the XGtd output. The top table shows the AWK-4131 radio's Wi-Fi specification regarding the symbol period and guard interval. By default, the radio uses a 400-ns inter-symbol guard time that can be increased to 800 ns. The bottom table lists the maximum excess delay from XGtd and the calculated delay spread for different antenna pairs and operating conditions.

One of the variables affecting the delay spread was the large ISS Thermal Control System (TCS) radiator next to Node 3. The TCS is normally outside of the view of the Node 3 antenna, but a few times per month, it may be moved into a position where it obstructs the path between ECOSTRESS and the Node 3 zenith antenna. In this case, the excess delay of the rays is altered. The delay spread for these two configurations (with and without TCS blocking) were computed. Notice that the delay spread values in either

case are well within the inter-symbol guard time and, therefore, ISI due to multipath is not an issue for the ECOSTRESS-to-Node 3 Wi-Fi link.

Table 4. Top: Moxa radio IEEE 802.11n specs. Bottom: delay spread values in ns for the ECOSTRESS-to-Node 3 Wi-Fi link with and without TCS blocking.

Parameter	Value	Comments
Channel bandwidth (MHz)	40	Bond two 20MHz channels
Number of carriers	128	52 subcarriers, 4 pilot, and 8 nulls per 20MHz
Bandwidth per carrier (MHz)	0.3125	
Symbol period (ns)	3200	$1/bandwidth\ per\ carrier$
Symbol period (ns) with default guard interval	3600	ECOSTRESS radio symbol period guard interval setting is 400 ns
Symbols period (ns) with larger guard interval	4000	Radio guard interval can be increased to 800 ns

ECOSTRESS-to-Node 3		Zenith-to-zenith	Zenith-to-nadir	Nadir-to-zenith	Nadir-to-nadir
RMS Delay Spread (ns)	LOS	17.35	4.77	17.66	2.05
	w/TCS	5.27	-	6.74	-
Max Delay Spread @ power ≥ -100 dBm	LOS	49.08	235.40	48.71	13.79
	w/TCS	33.95	-	55.04	-

IV. Link Budget

During the link design process, the mission's link budget went through many iterations as the telecom parameters became more well defined. A few months before launch, when the exact antenna locations and the WAP cable lengths were finalized, JSC released the final static link budget as shown in Table 5. In this table, the XGtd simulations were run with the most up-to-date parameters. JSC also performed additional experiments with the Node 3 WAP that showed the radio's MIMO threshold was -72 dBm, a couple of dBs lower than the Moxa radio's MIMO threshold. Based on the final link budget, the ECOSTRESS Wi-Fi link had a healthy margin in excess of 6 dB for all antenna pairings. The link budget and the multipath analysis together were used to satify mission requirements on the ECOSTRESS Wi-Fi link performance.

Table 5. Final link budget for the ECOSTRESS Wi-Fi link (courtesy of Chatwin Lansdowne, JSC). This is a point-to-point link budget without taken into account antenna diversity.

	EWC Static Link Margin (EcoSTRESS --> Node 3)							
	EcoSTRESS 1		**EcoSTRESS 2**		**EcoSTRESS 3**		**EcoSTRESS 4**	
Parameter	HR 0606	HR 0640	HR 0606	HR 0640	HR 0606	HR 0640	HR 0606	HR 0640	
1 Moxa transmit power	17	17	17	17	17	17	17	17 dBm
2 EcoSTRESS cable assembly loss	-3	-3	-3	-3	-3	-3	-3	-3 dB
3 Antenna gains, pointings, polarization, space loss (XGTD avg)	-64.4	-64.74	-63.61	-65.06	-67.05	-68.21	-64.31	-65.83 dB
4 Range	18.14	18.05	18.04	17.95	18.18	17.84	18.02	17.67 m
5 Frequency	5300	5300	5300	5300	5300	5300	5300	5300 MHz
6 Node 3 cable assembly losses (median expected)	-9.4	-11.1	-9.4	-11.1	-9.4	-11.1	-9.4	-11.1 dB
7 TRP	-59.8	-61.84	-59.01	-62.16	-62.45	-65.31	-59.71	-62.93 dBm
8 BelAir receiver sensitivity	-72	-72	-72	-72	-72	-72	-72	-72 dBm
9 **Link margin**	**12.2**	**10.16**	**12.99**	**9.84**	**9.55**	**6.69**	**12.29**	**9.07 dB**

V. Field Verification of Wi-Fi Link Analysis

Field Wi-Fi testing was conducted on the JPL Mesa to verify performance of the Wi-Fi link analysis. A mockup of the ECOSTRESS payload was built and identical copies of the TECOM flight antennas were mounted on payload antenna locations #1 and #2 as seen in Figure 35. The mockup models the RF signal reflections from the payload in flight. An unmodified commercial Moxa AWK-4131 radio was used to simulate the ECOSTRESS radio, and was connected to the TECOM antennas to transmit data. A mockup of the ISS Node 3 structure was not created due to cost and schedule, however the two receive WAP antennas were placed at same distance and look angle corresponding to flight configuration. The Myers antennas were not available to JPL so the BelAir radio and its factory default antennas were used to simulate the Node 3 WAP. Different attenuations were added at the antenna inputs of the BelAir WAP (identified as antenna connections #3 and #4) to simulate onboard cable loss that could be associated with different coaxial cable lengths between the WAP and the Node 3 antennas. At the time of the test, the exact location of the Node 3 WAP had not been determined and the coaxial cable run to the Node 3 antennas could have been tens of meters in the worst case. An illustration of the test configuration is shown in Figure 13.
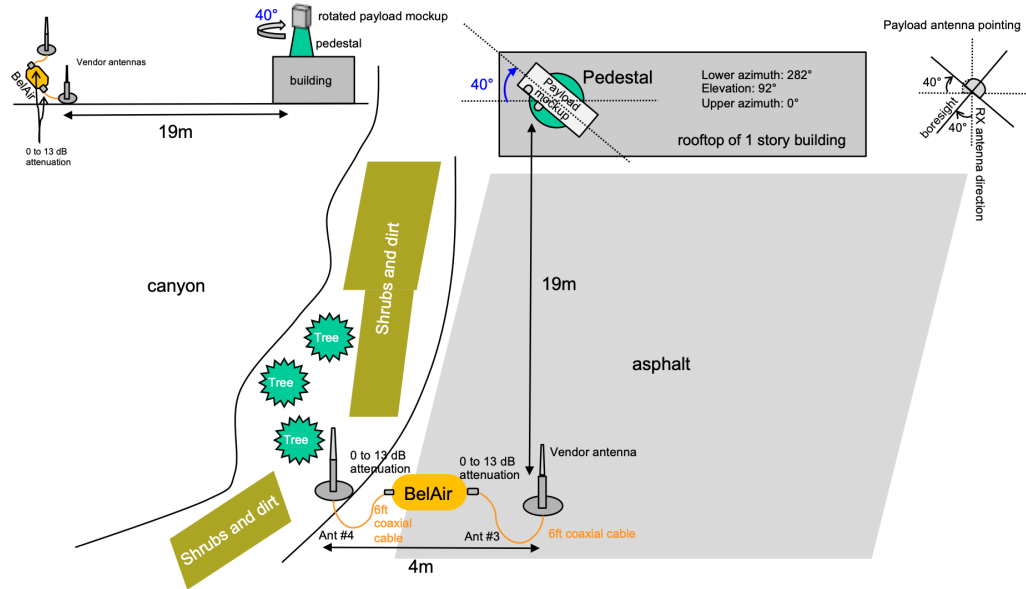

Figure 13. Wi-Fi field test configuration

Different antenna combinations and pairings were also tested to simulate SISO, MISO (Multiple-Input Single-Output), and MIMO. Both payload antennas were connected for MIMO and for MISO. Payload antenna #2 was disconnected for SISO. Figure 14 shows four plots of the measured throughput versus link power reported by the AWK-4131 radio. These four plots contain the same data, but are marked differently to illustrate different points. Figure 14(a) shows how the different BelAir antennas were connected and attenuated. The black "X"s mark the MIMO experiment where both of the BelAir WAP antennas were attached. The numbers in parentheses indicate the respective

antenna attenuations. The green circles mark the MISO experiment and the green triangles mark the SISO experiment where only BelAir antenna #4 was connected and the numbers in the parentheses indicate its input attenuation. The orange circles mark the MISO experiment and the orange triangles mark the SISO experiment where only BelAir antenna #3 was connected and the numbers in parentheses indicate its input attentuation. For the MIMO tests, the BelAir antennas were attenuated in different combinations of 0, 3, 10, and 13 dB. In MISO or SISO, the single BelAir antenna was attenuated by 0, 3, 10, or 13 dB.

Note that the MIMO threshold in Figure 14 is −70 dBm. If the link power is above this threshold, the radios would take advantage of antenna diversity to increase throughput. Figure 14(b) shows that just below this threshold the throughput values of the MIMO, MISO, and SISO antenna configurations are similar. Here, disconnecting BelAir antenna #3 did not seem to impact throughput very much, indicating the weakness of this antenna location since it is far away from the boresight of the payload antennas. Figure 14(c) shows that at or above the −70 dBm link threshold, the BelAir WAP radio used signals from both antennas. Less attenuation in the weaker BelAir antenna (#3) increased TCP throughput. And MIMO with no antenna attenuations gave the best received power reading and the best throughput as expected. Figure 14(d) traces out an envelope for the throughput curve. MIMO outperforms MISO and MISO outperforms SISO. By designing the link for a −70 dBm power requirement, ECOSTRESS Wi-Fi will support at least a 30-Mbps TCP/IP link to the ISS.
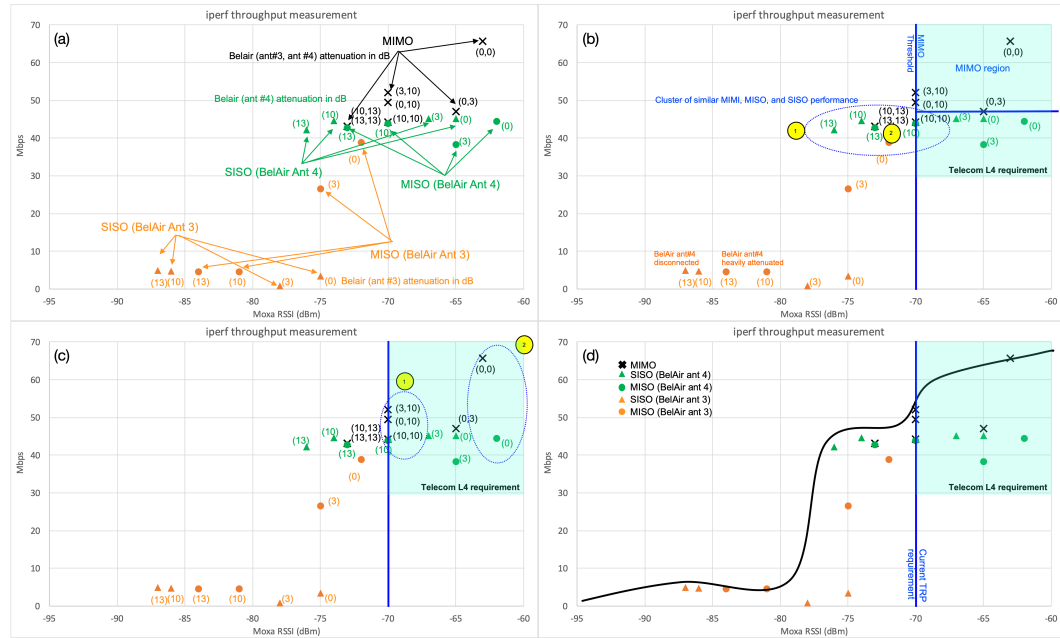

Figure 14. Field test Wi-Fi throughput

A. Diversity Combining in the BelAir WAP Radio

An additional SIMO (Single-Input Multiple-Output) test with one payload antenna and both BelAir antennas was performed in the same test setup to demonstrate that the BelAir radio does indeed implement antenna diversity combining. Figure 15 plots the different link power distributions logged by the two radios during different tests. The top plot is the received signal strength indicator (RSSI) logged by the AWK-4131 radio and the bottom plot is the RSSI logged by the BelAir WAP radio. The readings should be the same since the radios are logging the same link, but there is an offset between the two readings because the two vendors implemented the received signal strength estimators differently. For the same link, the AWK-4131 radio's received signal strength reporting is about 3 dB higher than the calibrated power measurement. The BelAir radio's received signal strength reporting is about 7 dB higher than the calibrated power measurement. A comparison of the SIMO peak reading (-63 dBm) to the SISO peak readings using BelAir antenna #3 (-75 dBm) and antenna #4 (-66 dBm) for the AWK-4131 radio shows that the BelAir radio is likely implementing a diversity technique similar to equal gain combining because $20 \log_{10}(\sqrt{10^{\frac{-75}{10}}} + \sqrt{10^{\frac{-66}{10}}}) = -63.36$. The same conclusion can be made using received signal strength readings from the BelAir radio since $20 \log_{10}(\sqrt{10^{\frac{-68}{10}}} + \sqrt{10^{\frac{-57}{10}}}) = -54.84$. With equal gain combining, the probability of closing the ECOSTRESS Wi-Fi link with at least 3-dB margin is close to 100% as shown in Table 3.
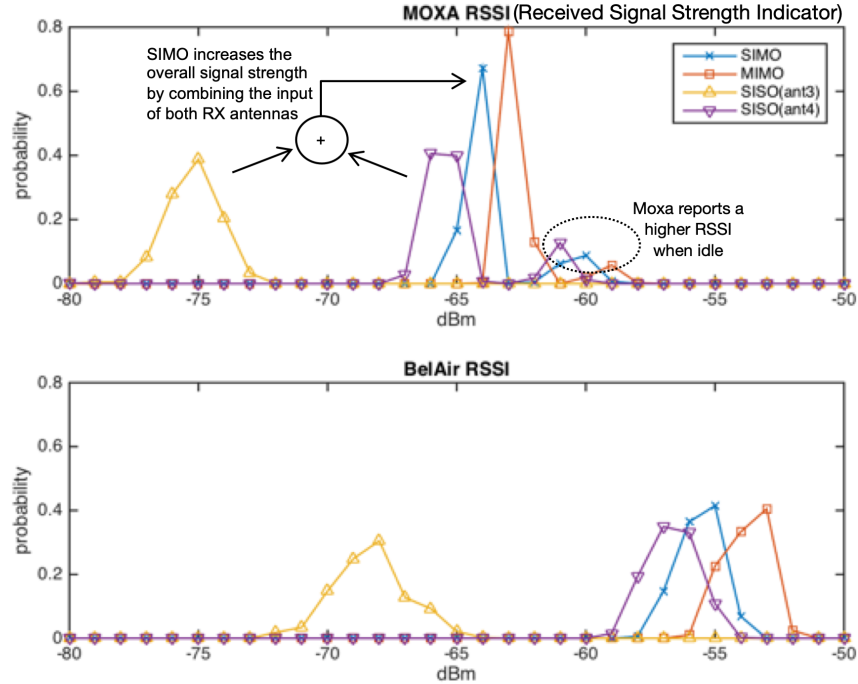

Figure 15. Antenna diversity combining in the BelAir radio.

B. Duration Testing

A 16-hour continuous transmission test was conducted in the field using the COTS AWK-4131. The Wi-Fi link was stressed by adding a 13-dB attenuator to each of the BelAir antennas. The result is shown in Figure 16. The blue line marks the measured data throughput during the test. The orange line shows the link rate reported by the AWK-4131 radio. Throughput was steady overall and averaged 43 Mbps, but did drop to zero during a brief outage between hours 7 and 8. However, this dropout was not important because it did not impact the overall link integrity. This long duration test gave confidence during the telecom design phase that the Wi-Fi link could be used continuously to downlink data for hours at a time.
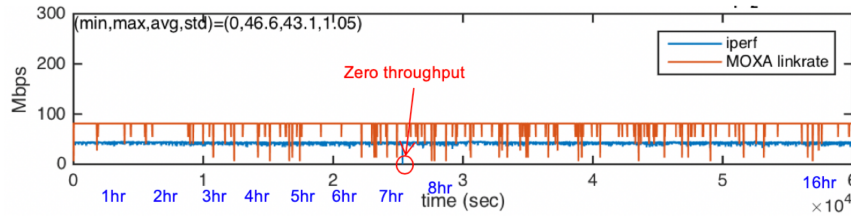

Figure 16. Continuous data transmission test

VI. Wi-Fi Electronics Box Assembly

The ECOSTRESS radio, called the Wi-Fi Electronics Box Assembly (WEBA), was designed to provide the W-Fi physical layer interface between the ECOSTRESS instrument and the ISS WAP. Its design centered on the use of COTS 802.11n radio boards that have been approved for use on the ISS. JSC provided several Moxa AWK-4131 Outdoor Industrial IEEE 802.11a/b/g/n IP68 Wireless AP/bridge/client units to ECOSTRESS as government furnished equipment (GFE). These commercial AWK-4131 units, originally designed for outdoor use such as on freight trains, had been upscreened by JSC and upgraded with a custom version of the firmware which increased the transmit power of the Wi-Fi boards. Radiation qualification testing of the AWK-4131 had been performed by JSC previously. Use of these ISS-approved COTS boards helped reduce costs and ensured compatibility with the ISS Wi-Fi Access Points.

The WEBA was designed for a minimum operating life of one year on the ISS. To provide robustness in the event of a component failure, the WEBA contained two independent AWK-4131 radio boards which were each connected to two of the externally mounted antennas (one on the nadir panel and the other on the zenith panel). During nominal operations, only one Wi-Fi board is powered on at a time and only the pair of antennas connected to that Wi-Fi board radiates This is necessary to minimize power consumption and to reduce the thermal load of the WEBA. In the event of a Wi-Fi board or antenna failure, a command can be sent to the WEBA to switch to the other AWK-4131 board and corresponding antenna pair.

As risk reduction, a breadboard model of the WEBA was built to be used for testing

and eventual delivery to the flight software (FSW) testbed. The breadboard model differed from the flight model in that it could either be powered via a 120 VAC input or an external +28 VDC supply. The breadboard model was used to validate assembly procedures and test procedures that would eventually be used on the flight WEBA model, and to verify performance of the ground support equipment (GSE). Figure 17 shows a picture of the breadboard WEBA along with the GSE mounted in the traveling case. The traveling case was needed when the breadboard unit was taken to JSC for an early end-to-end validation and verification test.
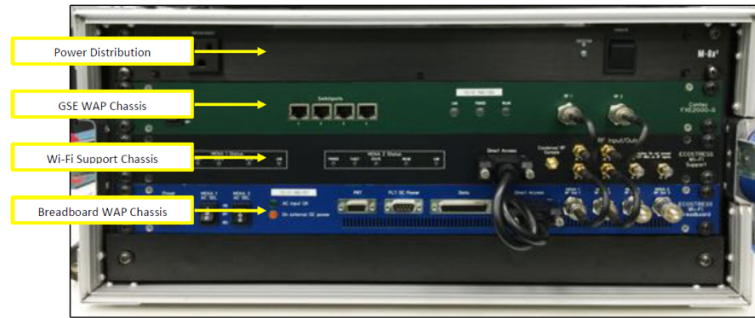
Figure 17. Breadboard WEBA and GSE

A. WEBA Design Trade Studies

The initial design of the ECOSTRESS WEBA included two AWK-4131 Wi-Fi radio boards connected to a COTS Ethernet switch, which interfaced to the ECOSTRESS CEU (Central Electronics Unit). The CEU would provide the data packets using Lightweight IP and the Ethernet switch would route the packets to the correct AWK-4131 radio board based on the IP address. Each AWK-4131 board had two RF outputs; one connected to the antenna on the zenith panel and the other connected to the antenna on the nadir panel. A pair of RF switches were used to control which antenna on the zenith and nadir panels were used, depending on which provided a better link. The RF switches also provided robustness in the event of a failure in one of the antennas.

However, one problem with the initial design was that the COTS Ethernet switch was a single-point failure, meaning that failure of the component could result in total loss of the Wi-Fi link. There was little reliability information on the Ethernet switch operating in a space environment. It also required a +5V DC power supply, which meant that a DC-DC converter module had to be added to convert the nominal +28V bus voltage to +5V. The selected DC-DC converter had flight heritage but was not in stock and was a long-lead part to order, which posed a schedule concern for the flight unit build.

A trade study was conducted which resulted in several changes to the initial design. The Ethernet switch was removed in favor of having the CEU directly control the routing of data to the AWK-4131 radio boards via separate data lines to each board. The CEU would select which data lines to send Ethernet data on, namely using the data lines connected to the active AWK-4131 board while the other board remained

powered off. This design allowed for removal of the COTS Ethernet switch and DC-DC converter from the WEBA design, but required each radio board to have a separate data connection to the CEU.

The second design trade involved the RF switches. Through the antenna field simulations, it was determined that a sufficient link to the WAP could be established using either of the low gain antennas on the zenith panel. The same was also true of the antennas on the nadir panel. Therefore it was not necessary to switch between the two antennas on either the zenith or nadir panels. The two RF switches were removed in favor of the simpler design where the antenna output ports from each AWK-4131 were directly connected to the LGAs on the zenith and nadir panels.

Figure 18 shows the initial WEBA design with the COTS Ethernet switch and RF switches, while the final simplified design is shown in Figure 19. As a result of the design modification, the mass of the WEBA was reduced by 1.88 kg (roughly 30%) and the WEBA power consumption was reduced by 6 Watts (roughly 40%) compared to the initial design. In addition, the overall reliability was increased and the size of the WEBA enclosure was reduced. The electrical interference with the CEU was slightly more complex because of the data lines to both AWK-4131 radio boards, but this was partly offset by the removal of the electrical pulsed signals from the CEU previously used to control the RF switches.
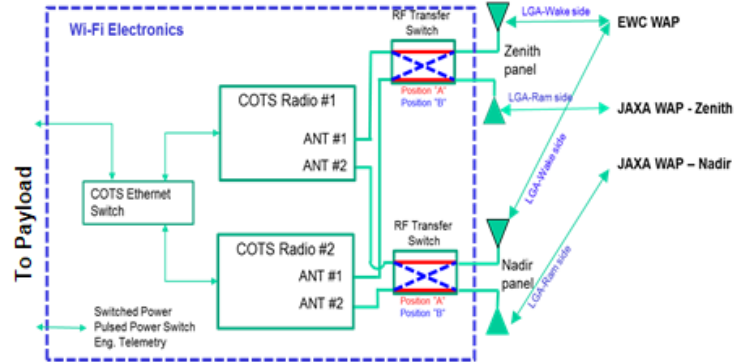

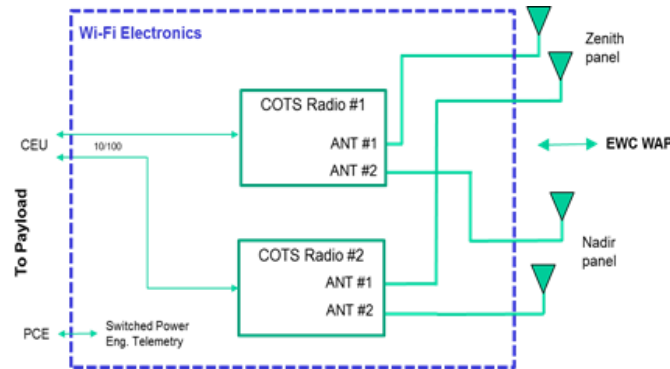Figure 18. Block Diagram of the Initial WEBA Design.

Figure 19. The final WEBA Design.

B. WEBA Thermal Design

The use of commercial AWK-4131 boards originally intended for terrestrial applications created several challenges for the WEBA design. One of the primary design challenges was how to deal with thermal dissipation. The COTS AWK-4131 thermal design relied primarily on thermal convection via airflow to keep the electronic components on the radio boards cool, which could not be applied for the WEBA in a space environment. The thermal dissipation in vacuum only came via the steel mounting bolts and brass spacers attaching the radio boards to the WEBA aluminum enclosure, which provided a heat conduction path to the base plate. The base plate itself is mounted to the ECOSTRESS Y-panel which is actively cooled using heat pipes.

The driving WEBA thermal design constraints were (1) to not exceed the derated junction temperature limits of the AWK-4131 board components during nominal Wi-Fi operations, and (2) to survive the fault case where both AWK-4131 boards were powered on simultaneously for one hour. Of particular concern for the WEBA thermal design was the RF daughter card mounted on the topside of the AWK-4131 radio board, which carried a number of high power electronic components including the dual band 802.11n LAN front-end chip and the Atheros MIMO chip. On the bottom of the radio board, the Cavium processor chip and the Vitesse Ethernet PHY layer chip were also high-power dissipators.

In order to meet the thermal constraints of the WEBA, the thermal design needed to provide a heat conduction path from high-power dissipating components on the topside and bottomside of the AWK-4131 board to the WEBA enclosure base. The design solution was to add a copper thermal strap from the RF daughter card to the base plate, and to add a thermal gap filler layer to provide a heat conduction path between the bottom of the AWK-4131 board and the base plate. In addition, the mounting screws for the daughter card was lengthened compared to the COTS design so that they extended all the way to the base plate. Additional brass standoffs were added to provide further heat conduction paths from the daughter card to the base plate. The thermal gap filler chosen was Parker Chomerics Therm-A-Gap 579G, which is a compressible heat-conducting foam-like material and had previously been used on the Mars Science Laboratory rover. Figure 20 shows a cross-section view of the thermal design used to dissipate heat from the RF daughter card and radio board. The strap and the bracket were made of copper, and a thin layer of thermal gap filler was added on top of the RF daughter card to improve heat conductivity to the bracket.
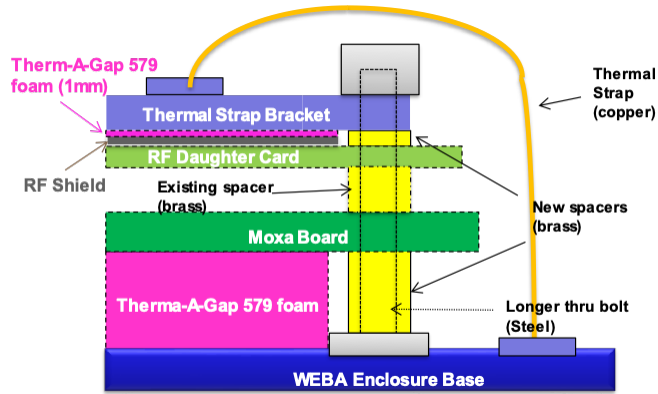
Figure 20. **Thermal strap and bracket design for RF daughter card heat dissipation.**

The WEBA thermal performance analysis [5] was performed by Orbital ATK under a MEDALS (Multi-divisional Engineering, Design, Analysis Lab-wide Support) contract. Figure 21 shows a plot of the predicted temperatures at the bottom of the AWK-4131 board, while Figure 22 shows the temperature profile of the RF daughter card with and without the thermal strap.
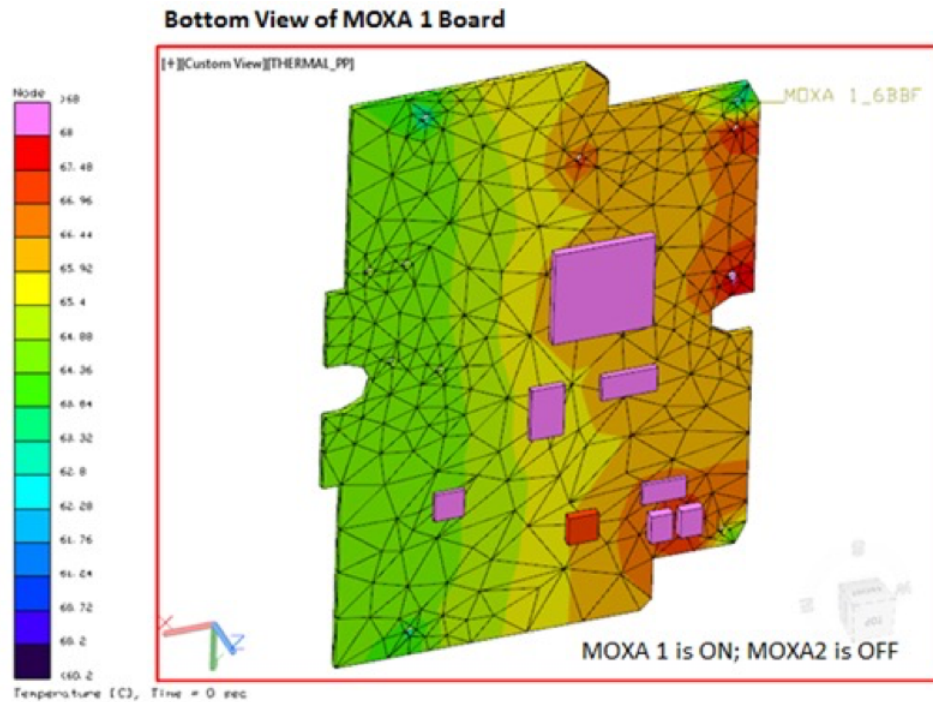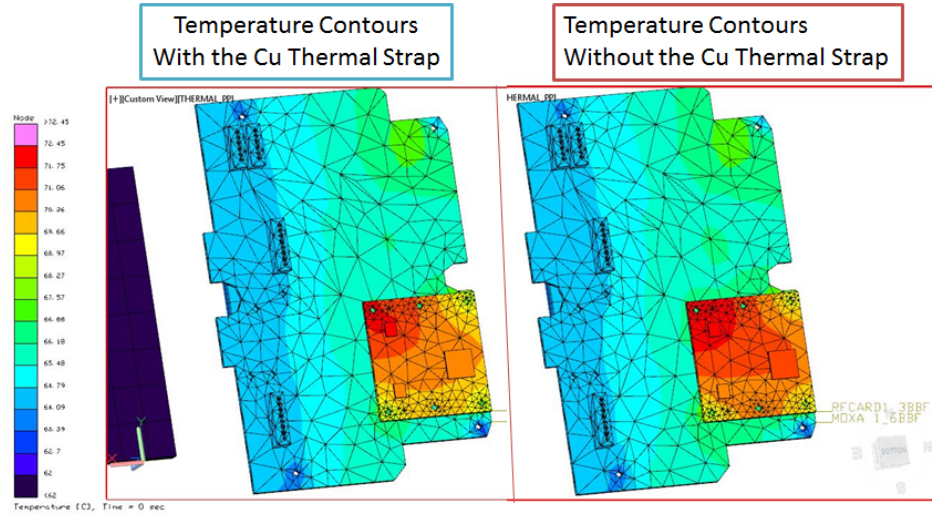

Figure 21. Temperature from bottomside of AWK-4131 board at +60°C panel boundary (hot condition).

RF Daughter Card (MOXA 1)

Figure 22. Temperature of RF daughter card with (left) and without (right) thermal strap at +60°C panel boundary.

One of the difficulties in evaluating the thermal design was the lack of information about some of board components on the commercial AWK-4131 board. The maximum allowed junction temperatures of some of the components were not available, so junction temperature limits were estimated based on specifications from similar components or from the maximum case temperature instead. Thermal conduction through the different layers of the AWK-4131 board was assumed based on rough estimates of the copper content in the Gerber files of the printed circuit board provided by the manufacturer. Due to the uncertainty introduced by the assumptions made in the analysis, a number of test thermocouples were added to the inside of the WEBA to verify the thermal design performance during thermal vacuum (TVAC) testing at hot and cold flight allowable temperature limits. Since removal of the test thermocouples required disassembly of the WEBA, the decision was made to leave the test thermocouples in the WEBA but to cut the wire leads following the conclusion of TVAC testing.

C. Mechanical Stress Analysis

Mechanical stress analysis [6] using a finite element model of the WEBA was also performed by Orbital ATK, including random vibration analysis, quasi-static analysis, and shock analysis. The addition of the thermal gap filler foam below the AWK-4131 board helped attenuate the fundamental mode of the printed circuit board, and the thermal bracket did the same for the RF daughter card. Vibrations at the fundamental mode frequency is critical because it results in large displacements in the circuit board that can cause fatigue damage to solder joints, lead wires, and pin connections of the chip components.

The mechanical stress analysis showed that the results of all modes were above 100 Hz. The first mode of the WEBA was of the enclosure cover at 309 Hz, and the second mode was of the RF daughter card at 514 Hz. All stress cases showed a positive margin of safety.

D. WEBA Electrical Interfaces

The WEBA receives the payload data and commands from the ECOSTRESS CEU via a 25-pin data connector. Signaling between the WEBA and CEU conforms to the IEEE 802.3 Ethernet specification. In addition to the Ethernet signals, the 25-pin data connector includes analog health and status signals from the AWK-4131. These analog signals are sampled by the Housekeeping Unit (HKU) in the CEU, and are derived from the voltages that drive the LED status lights in the commercial AWK-4131 enclosure. These voltages are used to determine if the unit is powered on, whether there is an active WLAN connection, if there is a fault or IP conflict, and whether a AWK-4131 reboot is in process. The power connector carries two +28V DC bus voltage lines from the Power Control Electronics (PCE) module, one to each AWK-4131 board. These bus voltage lines are used to power on and off the AWK-4131 boards. There is also a Direct Access port used for testing and debugging purposes, but this port was terminated before the ECOSTRESS launch. Figure 23 shows the D-sub connector interfaces on the side of the flight WEBA. The cables coming through the vent holes are for the thermocouples used to monitor the AWK-4131 component temperatures during TVAC testing, and were also removed prior to flight integration with ECOSTRESS.
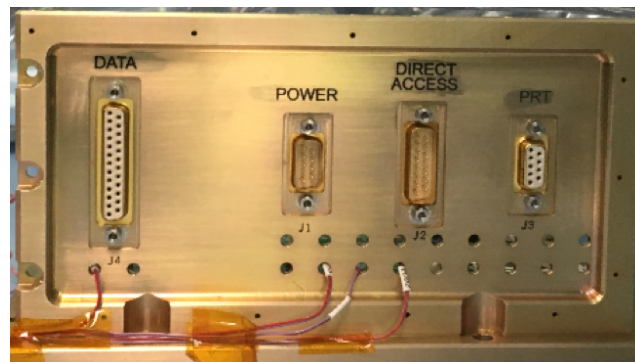

Figure 23. WEBA D-sub connector Interfaces.

E. WEBA Manufacturing and Assembly

The Moxa AWK-4131 radios from JSC arrived in the original COTS enclosure, shown in Figure 24 on the left. After the shipping inspection, an acceptance test at JPL was performed to verify that the Wi-Fi radio was operating correctly. Then the AWK-4131 board was removed from the COTS enclosure using the disassembly procedure originally developed and tested for the breadboard WEBA unit. The units delivered from JSC were identical to the commercial version, except the optical connectors had

been removed and a conformal coating had been applied to the board. In addition, a new firmware had been loaded which increased the maximum output RF power and fixed a problem with Wi-Fi Channels 52/56. The AWK-4131 Wi-Fi board after removal from the COTS enclosure is shown in Figure 24 on the right.

Figure 24. Left: Moxa AWK-4131 COTS Enclosure. Right: AWK-4131 Wi-Fi board after disassembly.

Figure 25 shows the overall flow diagram for the WEBA manufacturing and assembly. The majority of the assembly was done at JPL in Building 103. As shown in the diagram, the Molex power and data connectors were next removed from the board since they were not suitable for space flight. In addition, the 16-pin header connected to the status LEDs on the outside of the COTS enclosure (Power, State, Fault, WLAN, and LAN) was removed. The auxiliary board carrying the status LED was discarded. The voltages used to drive the LEDs were re-routed via data lines to the HKU of the CEU. The HKU sampled these voltages to provide the status of the Wi-Fi board similar to what was provided by the LEDs in the original COTS enclosure.

Following disassembly of the radio boards, an aluminum enclosure was built for the WEBA to hold the two AWK-4131 boards. The WEBA box cover, walls, and base were
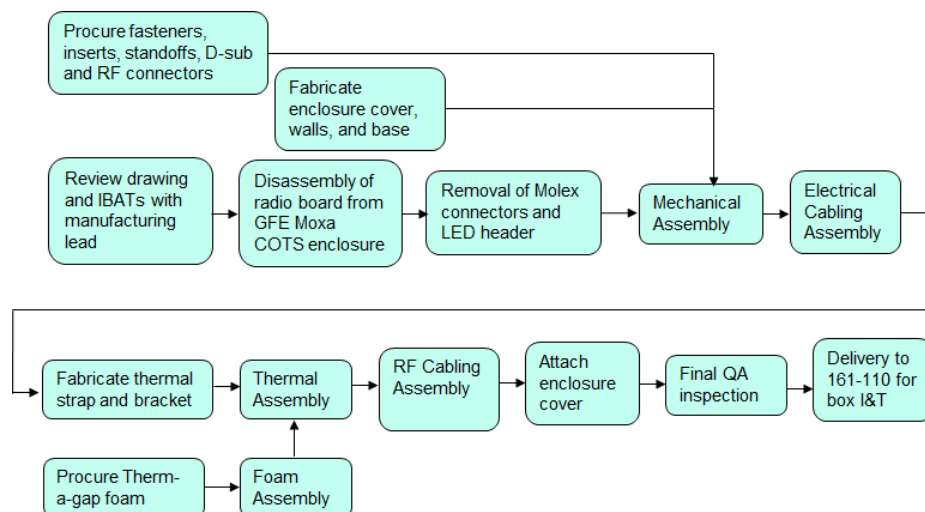
Figure 25. Flow diagram of WEBA manufacturing and assembly.

individually fabricated and then assembled together. After mechnical assembly, the enclosure was painted with a gold paint. Four D-sub connectors were added on the side of the WEBA enclosure for the Data, Power, Direct Access, and platinum resistance thermometers (PRT) connections. The Direct Access connection was only used during ground integration and test, and was disconnected in the final flight configuration. Vent holes were also added to the side of the WEBA enclosure. Four Threaded Neill—Concelman (TNC) coaxial connectors were placed on the outside of the WEBA for each of the antenna RF outputs from the AWK-4131 boards. Finally, the AWK-4131 radio boards attached to the base of the enclosure by using a series of brass spacers placed at the holes drilled in the base plate which correspond to mounting holes for the original COTS enclosure. A drawing of the exterior of the assembled WEBA box is shown in Figure 26 along with its dimensions.
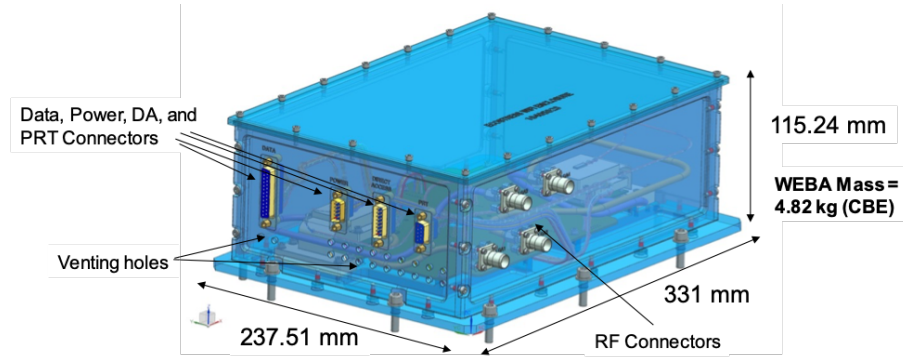

Figure 26. Computer-aided design (CAD) drawing of WEBA enclosure.

After the mechanical assembly was completed, the electrical connections were made. During electrical cabling assembly, the power and Ethernet connections were directly soldered onto the board and routed to the D-sub connectors. The connections for the LED status signals were also soldered directly on the board. The RF outputs of the daughter card on the radio boards were connected to the external antenna TNC connectors using coaxial cables. Figure 27 shows how the RF cables were routed inside the WEBA enclosure. It also provides a top-view drawing of the inside of the WEBA box along with the orientation of the two AWK-4131 boards.
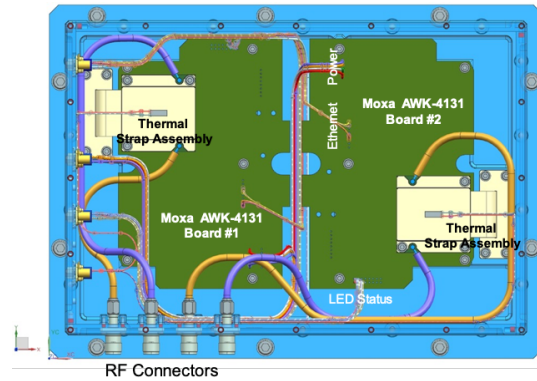

Figure 27. CAD drawing of WEBA enclosure (top view).

During the thermal assembly process, a bracket was manufactured and added to mechanically support the copper thermal strap attachment to the RF daughter card. The Therm-a-gap foam was added between the bottom of the radio board and the base plate of the enclosure. Because the components on the bottom of the AWK-4131 board had varying heights that exceeded the vendor-recommended foam compression percentage of between 20–40% for optimum thermal contact, thermal 579G foam of three different thicknesses (from 2.5 mm to 7 mm) was ordered and cut to fit the height profile between the base plate and the bottom of the Wi-Fi board. Two PRTs were added to monitor the temperature of the AWK-4131 RF daughter cards in flight, as well as a number of test thermocouples for use during TVAC testing. As part of the thermal design, a total of 10 extra steel mounting bolts were used to attach the WEBA base to the ECOSTRESS Y-panel and a thermal paste was added in order to obtain better thermal conduction during final integration of the WEBA to the Y-panel.

F. Thermal Gap Filler Issue

During manufacturing, there was concern about contamination and outgassing from the thermal gap filler based on previous MSL experience. As a result, an extended bakeout of the thermal gap filler was recommended which was performed prior to assembly. However, during final assembly of the WEBA, small amounts of a silicon oily residue was noticed extruding from the thermal gap filler when it was compressed. Due to concern about potential contamination of the manufacturing lab and to other projects in the lab by the silicon oil, the WEBA was moved to a different facility where the final assembly was completed. The silicon residue was cleaned off and did not impact the performance of the WEBA. Figure 28 shows a picture of the inside of the WEBA during final assembly, before the enclosure cover had been attached.
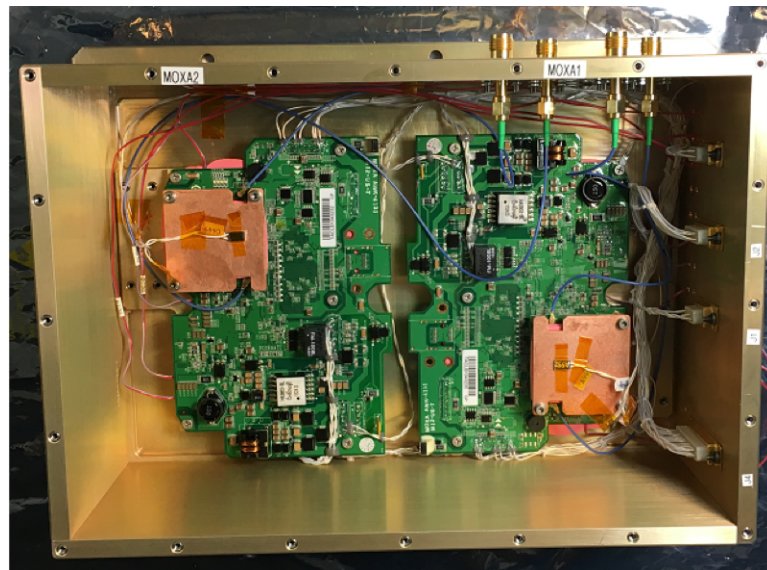

Figure 28. Interior of assembled flight WEBA.

VII. Environmental and Functional Testing

A. WEBA Functional Testing

An initial functional test of the WEBA was performed after final assembly of the radio. The functional test [7] was used to verify the (1) WEBA RF output power, (2) RF spectrum, (3) Simple Network Management Protocol (SNMP) commands used to configure the AWK-4131 radio boards, (4) dataflow over the Wi-Fi RF link, (5) configuration of network parameters, and (6) telemetry status signals from the WEBA. This functional test procedure was repeated at various stages of environmental testing to verify the performance of the WEBA.

B. WEBA Random Vibration Testing

Following the initial functional test, random vibration testing was conducted with the WEBA at JPL. The WEBA was placed on the shaker table, and random vibe levels in all three axis were execute in accordance to the ECOSTRESS Environmental Requirements Document (ERD) [8]. Figure 29 shows a picture of the WEBA during random vibration testing.

A functional test of the WEBA Wi-Fi radio was performed after the random vibration testing was completed, to ensure that the WEBA performance had not been degraded by the mechanical vibration. A comparison of the pre- and post-vibe functional test results confirmed that there was no change.
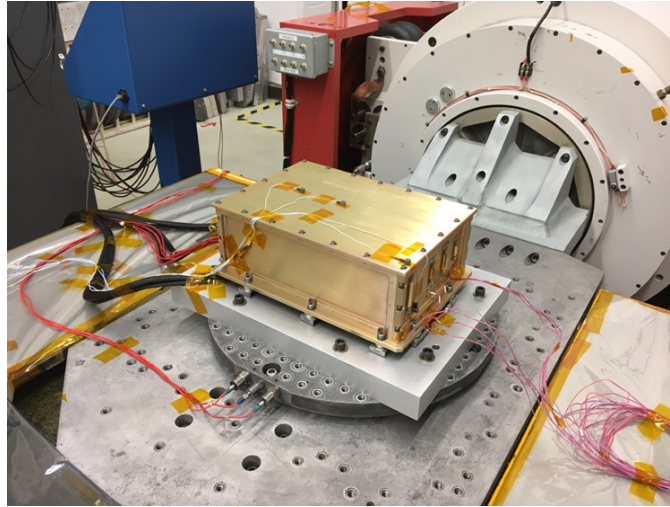

Figure 29. WEBA configuration during vibration testing.

### C. WEBA Electromagnetic Compatibility (EMC) Testing

Electromagnetic compatibility testing of the WEBA was performed at JPL. Both radiated susceptibility and radiated emissions testing were performed over the span of several days. The radiated emissions met the limits specified in the ERD and by the

ISS requirements documents, while the WEBA performance showed no anomalies during the radiated susceptibility testing.

D. WEBA Thermal Vacuum (TVAC) Testing

The ECOSTRESS telecom subsystem (not including the four Wi-Fi antennas) was tested in a thermal vacuum chamber from October 11–16, 2016. TVAC testing was performed in ETL Chamber 13 in Building 144. The telecom elements tested inside the chamber included the WEBA and the four flight RF cables internal to the payload, but not the four Wi-Fi antennas and the four RF cables external to the payload. A block diagram of the TVAC test configuration is shown in Figure 30.
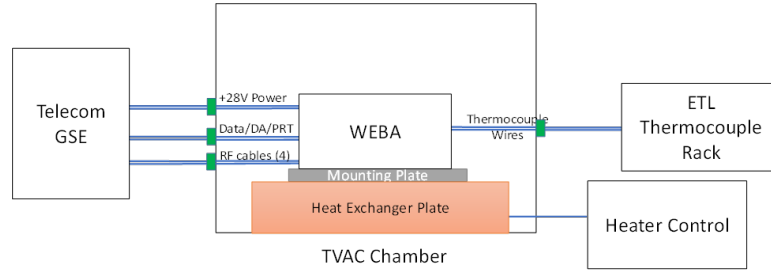
Figure 30. WEBA TVAC test configuration

The telecom hardware was put through three full thermal cycles over the Wi-Fi electronics Protoflight/Qualification temperature range (see Figure 31), as specified in the ECOSTRESS ERD. The temperature range with the WEBA in operation during the TVAC test was from $-5°$C to $+60°$C, and the non-operating temperature range (i.e., WEBA was powered off) was from $-35°$C to $+70°$C. Pressure inside the chamber during vacuum testing was less than 1×10^{-5} torr, as per ERD requirements. Figure 32 shows the WEBA inside the TVAC chamber prior to the start of the test.

Functional testing of both AWK-4131 boards per the WEBA Functional Test Procedure [7] was performed during the hot and cold operating temperature dwells ($+60°$C and $-35°$C), while mini-functional tests were conducted at intermediate temperatures ($+10°$C, $+25°$C and $+40°$C). Mini-functional tests were subsets of the full functional, mainly omitting some of the RF output power and spectrum measurements in the full functional test procedure. Both tests verified TCP and UDP data transfer, RSSI calibration, Ethernet interface, power on/off, data throughput, and SNMP commanding. The time needed to complete a functional test was roughly one hour per Moxa radio, and approximately 40 minutes for a mini-functional. In addition to tests in vacuum, a pre- and post-TVAC functional test was conducted at ambient temperature and pressure ($22°$C and one atm).
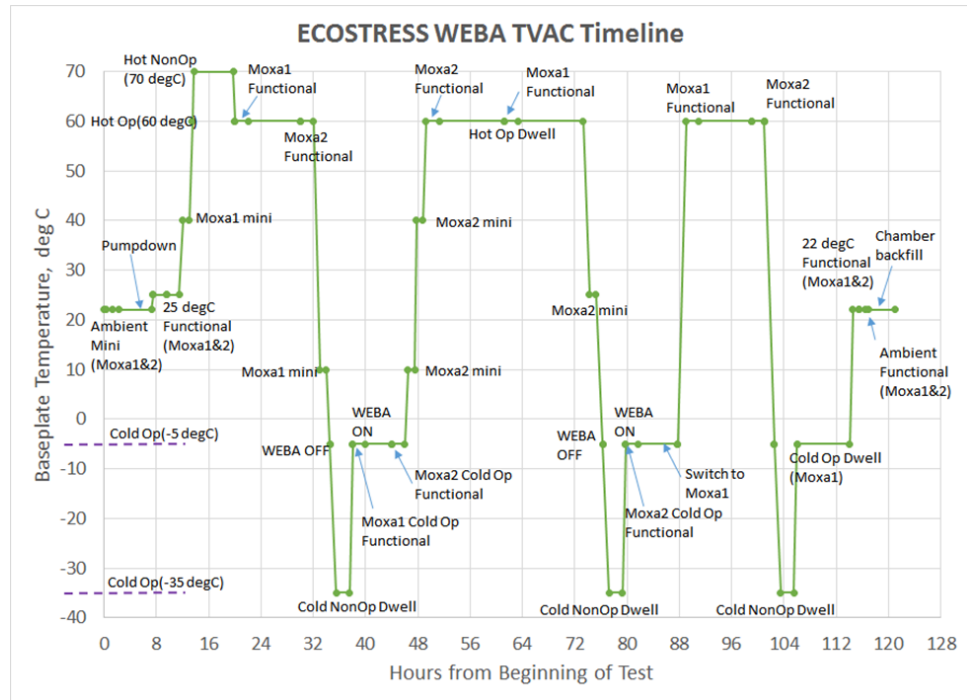
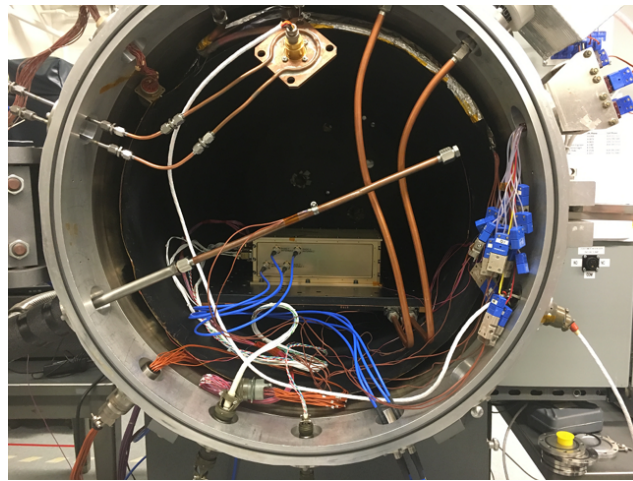**Figure 31. Temperature cycling for WEBA TVAC test**

Figure 32. WEBA placement inside TVAC chamber

Of particular interest during TVAC testing was the performance of the COTS AWK-4131 boards at the operating temperature extremes in vacuum. Figure 33 shows a plot of the RSSI calibration for Moxa1 board performed at multiple temperatures. The calibration curve is fairly linear and consistent over temperature, but had a slight offset compared to the actual measured RF power level at the WAP input. Figure 34 shows the WEBA data throughput measured by iperf, a software tool used to analyze network performance during Wi-Fi testing, as a function of the RF input power to the WAP. The results indicated that the throughput performance was relatively independent of temperature and met the ECOSTRESS data rate requirement at all temperatures.

The Wi-FI radios (Moxa1 and Moxa2) successfully passed all TVAC tests, and a number of telecom subsystem functional requirements were verified. Pre- and post-TVAC functional tests at ambient showed no significant changes in the Wi-Fi hardware performance after environmental testing. During TVAC testing, there were some issues caused by GSE software, but these were known a priori and did not affect the outcome of the TVAC test.
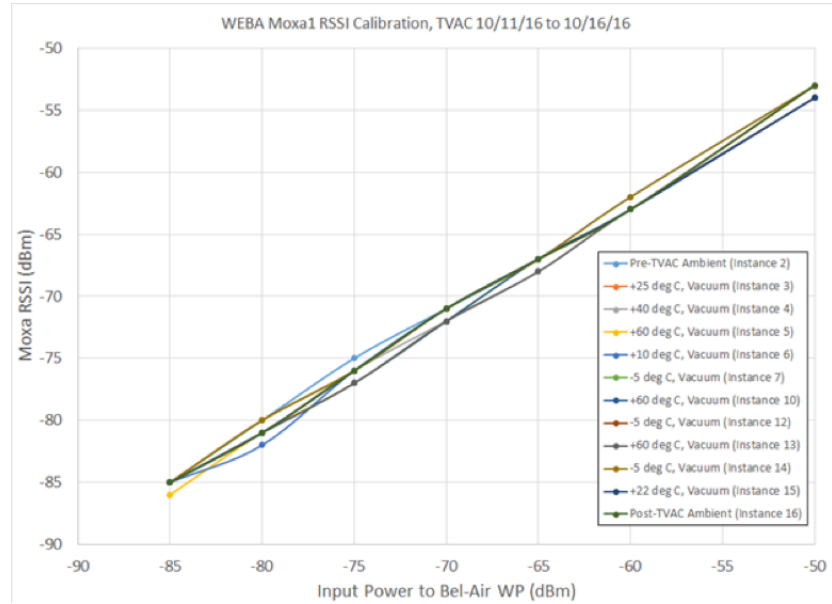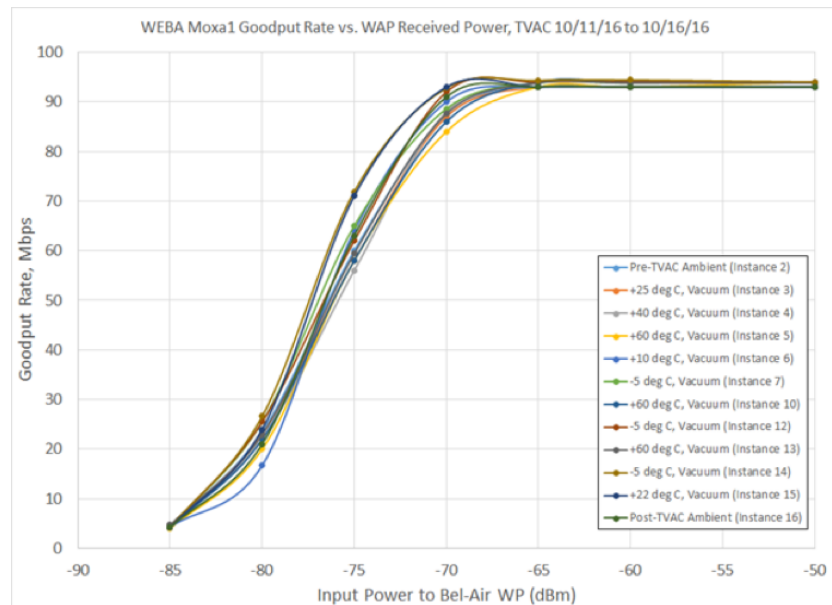

Figure 33. Moxa1 RSSI calibration

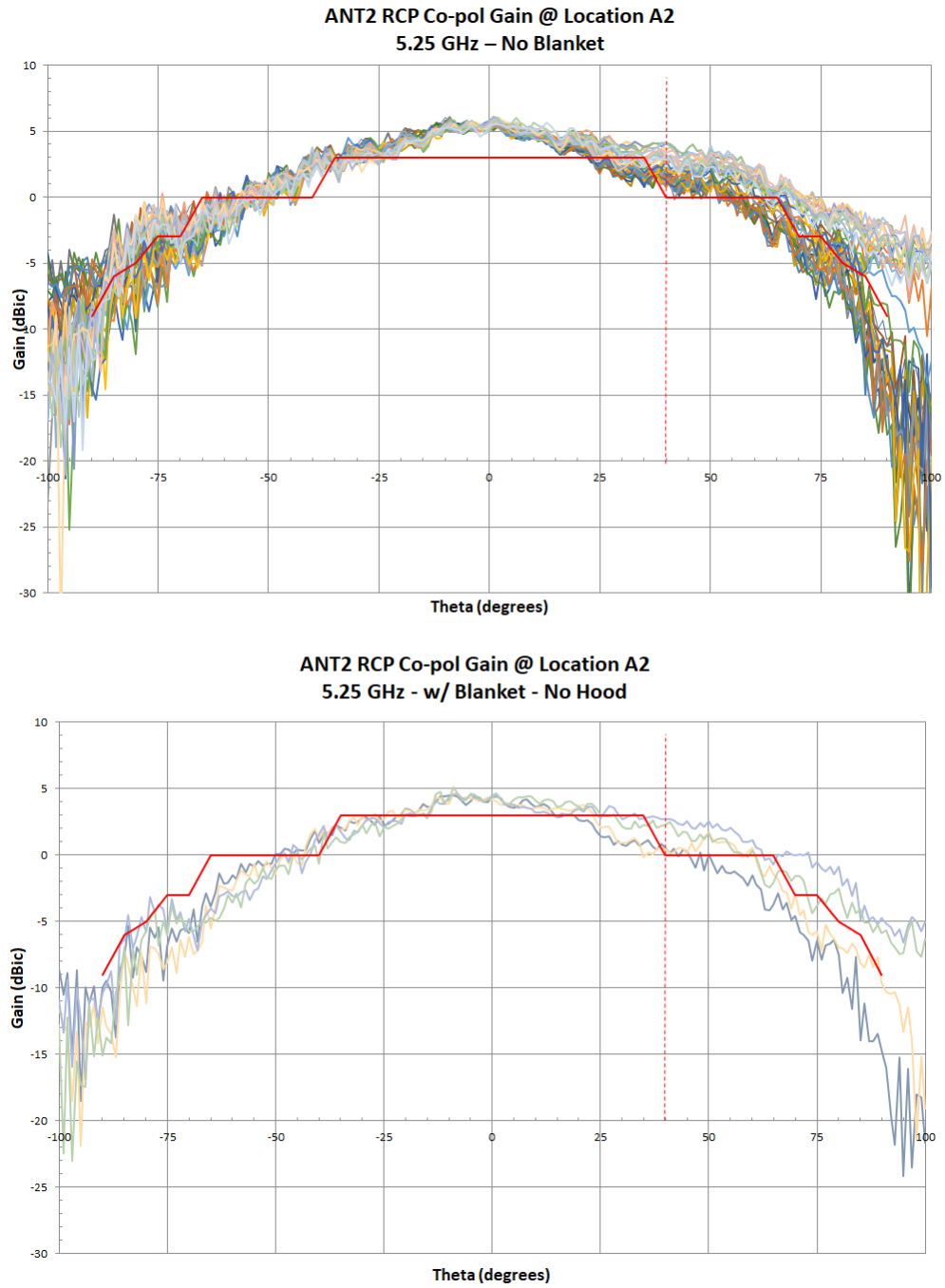**Figure 34. Moxa1 data throughput rate vs. WAP received power**

E. Wi-Fi Antenna Test with Thermal Blanketing

For thermal reasons, the ECOSTRESS payload is covered using a multi-layer insulation (MLI) blanket made of beta cloth (a woven silica fabric with Teflon coating). However the RF impact of covering the Wi-Fi antennas with beta cloth was unknown. To answer the question of possible RF impact, measurements of the ECOSTRESS Wi-Fi antenna pattern were made on the JPL Mesa Antenna Range. The TECOM Wi-Fi antennas were mounted onto the ECOSTRESS payload mockup using the flight antenna brackets (see Figure 35). The antenna gain pattern was then measured using three different configurations: (1) without any thermal blanketing covering the Wi-Fi antennas; (2) with the Wi-Fi antennas covered in beta cloth; and (3) with Kapton-Germanium windows inserted in place of the beta cloth over the Wi-Fi antennas.

Figure 35. Wi-Fi antenna gain test with ECOSTRESS payload mockup and MLI blanket

Figure 36 shows a comparison of the measured TECOM antenna pattern at 5.25 GHz with and without the beta cloth. The boresight antenna gain of the antenna was reduced by approximately 1.5 dB after being covered by the beta cloth. Using the Kapton-Ge window improved the antenna gain slightly, but was still about 0.5 to 1 dB less compared to the antenna gain without the beta cloth. In the final design, a decision was made not to cover the ECOSTRESS Wi-Fi antennas with beta cloth.

ANT2 RCP Co-pol Gain @ Location A2
5.25 GHz − No Blanket

ANT2 RCP Co-pol Gain @ Location A2
5.25 GHz - w/ Blanket - No Hood

Figure 36. Antenna gain pattern (ANT2) on mockup without blanket (top) and with beta cloth blanket (bottom).

VIII. Conclusion

A. Lessons Learned

Some of the lessons learned during the design, manufacturing, and testing of the ECOSTRESS Wi-Fi telecom subsystem:

1. Reliability and thermal analysis of COTS boards and components, especially if they have not previously been used in a space environment, can be difficult due to lack of information from the vendors. Expect to have to deal with lots of uncertainty/risk in the analysis and to do extra testing to build confidence in the analysis results.

2. Be careful when handling G579 thermal gap filler foam after thermal bakeout to avoid possible silicon oil contamination. Despite reading about the issues with the gap filler experienced by MSL, it was still an issue during the WEBA assembly.

3. Checkout and debugging of procedures on the breadboard unit made the manufacturing and assembly of the flight WEBA much smoother.

4. When dealing with COTS electronics, look out for components with gold-plated end caps which can affect the solder joints. For the WEBA, the fuses with gold-plated end caps had to be removed and replaced.

5. The conformal coating applied to the AWK-4131 boards had room-temperature-vulcanizing (RTV) silicone resin which should be avoided due to outgassing concerns. Also, after bakeout, the conformal coating exhibited microscopic cracking on the surface.

B. Telecom Subsystem Delivery and Current Mission Status

Following successful conclusion of environmental testing and the Hardware Review Certification Record (HRCR), the Wi-Fi telecom subsystem including the flight WEBA, the RF cables, antenna brackets, and antennas were delivered to the ECOSTRESS project. The telecom subsystem was integrated onto the Y-panel, and successfully passed instrument environmental and pre-launch testing.

ECOSTRESS was launched to the ISS on June 29, 2018. It was installed on the outside of the ISS at Site 10 of the JEM-EF (see Figure 37), and came online in July 2018. During initial on-orbit checkout (IOC), the payload achieved an excellent Wi-Fi connection with the ISS Node 3 WAP. A snapshot of telemetry from the WEBA radio 1 taken during IOC (as seen in Figure 38) showed that the established link power was -55 dBm and the transmission link rate was 300 Mbps, which is the maximum link rate supported by the AWK-4131 radio. The Wi-Fi link connection is strong enough to support MIMO communications. Since IOC, the WEBA has been running for 18 months almost continuously without encountering any issues or degradations in transmission rate. The hope is that future missions requiring a link to the external ISS Wi-Fi

network will consider using the WEBA 802.11n radio, which is space-qualified and has proven flight performance with ECOSTRESS.
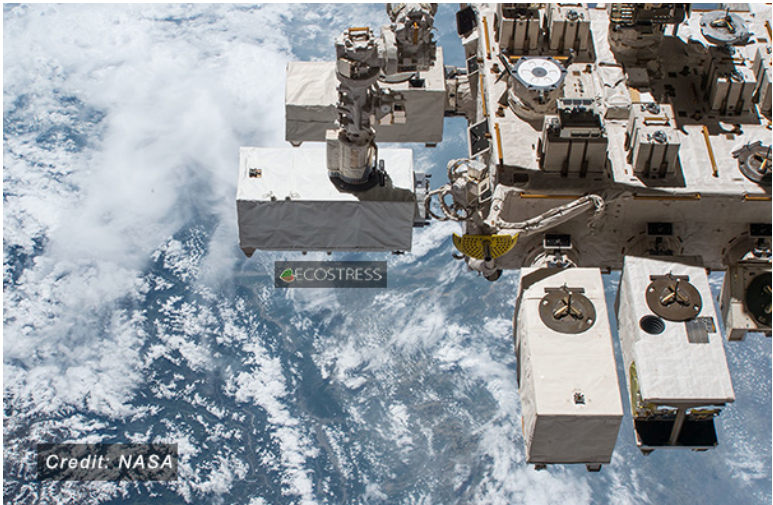

Figure 37. A picture of ECOSTRESS during installation to the JEM-EF. The Wi-Fi antennas are visible on the side of the payload.

Operation mode	Client
Channel	56
RF type	N Only (5GHz)
SSID	ISS_EXT_Payload_5GHZ
MAC	00:90:E8:3E:3D:C3
Security mode	WPA2
Current BSSID	00:0D:67:1E:5D:73
Signal strength	(-55dBm)
Transmission rate	300Mb/s
Current Transmission Power	20 dBm

Figure 38. A snapshot of the Moxa radio's wireless link status during initial on-orbit checkout.

To date, the ECOSTRESS mission has collected terabytes of science data from all continents and over a large portion of the oceans. The mission has also covered major events such as wildfires in the Amazon forest, historic heatwaves in Europe, and droughts in Costa Rica. In August 2019, the ECOSTRESS mission was extended for a second year. ECOSTRESS data is available online for the public [9]. NASA has also announced grants for scientists to process and use ECOSTRESS data. Over the next year and more, the ECOSTRESS mission will continue to monitor plant health and provide vital information of water use on Earth and to collect valuable thermal data with application to many other fields of Earth science.

References

[1] S. Hook et al., "ECOsystem Spaceborne Thermal Radiometer Experiment on Space Station," *JPL Critical Design Review (CDR)*, Pasadena, CA, March 8, 2016.

[2] M. Cheng et al., "ECOSTRESS Project Telecom Subsystem Functional Requirements Document," PDMS JPL D–94618, November 9, 2016.

[3] CCSDS, Low-Complexity Lossless and Near-Lossless Multispectral and Hyperspectral Image Compression. Blue Book. Issue 2. CCSDS 123.0-B-2. February 2019.

[4] CCSDS, CCSDS Bundle Protocol Specification. Blue Book. Issue 1. CCSDS 734.2-B-1. September 2015.

[5] M. Russell, "ECOSTRESS Wi-Fi Electronics Unit Thermal Design & Analysis - Revision 3," Interoffice Memorandum, April 7, 2016.

[6] J. Manash, "ECOSTRESS Wi-Fi Electronics Box Stress Analysis," ATK-RPT-1250, August 5, 2016.

[7] D. Lee et al., "Wi-Fi Electronics Box Assembly (WEBA) Functional Test Procedure," PBAT ID P10753, November 7, 2016.

[8] B. Kartolov, "ECOSTRESS Environmental Requirements Document," JPL D-94065, Rev C, October 17, 2016.

[9] https://ecostress.jpl.nasa.gov/

JPL CL#20-0858